Journal of Power Sources 204 (2012) 168–176

Contents lists available at SciVerse ScienceDirect

Journal of Power Sources

journal homepage: www.elsevier.com/locate/jpowsour

Effects of composition-dependent modulus, finite concentration and boundary constraint on Li-ion diffusion and stresses in a bilayer Cu-coated Si nano-anode

B. Yang[a,*], Y.-P. He[b], J. Irsa[c], C.A. Lundgren[d], J.B. Ratchford[d], Y.-P. Zhao[b]

[a] Department of Mechanical and Aerospace Engineering, University of Texas at Arlington, Arlington, TX 76019, United States
[b] Department of Physics and Astronomy, and Nanoscale Science and Engineering Center, University of Georgia, Athens, GA 30602, United States
[c] Department of Geology and Geophysics, University of Wyoming, Laramie, WY 82071, United States
[d] Army Research Laboratory, Adelphi, MD 20783, United States

ARTICLE INFO

Article history:
Received 7 November 2011
Received in revised form
25 December 2011
Accepted 1 January 2012
Available online 9 January 2012

Keywords:
Boundary constraint
Diffusion induced stress
Finite concentration
Lithium ion battery
Composition-dependent modulus
Stress assisted diffusion

ABSTRACT

During the lithiation of a Si anode from pure Si to fully lithiated alloy, the volume expands four times and modulus varies by several tens of times. Thus, the Li-ion diffusion and the stress evolution can be strongly coupled, which may play a significant role in determining the anode performance. In this work, we present a theoretical study of the fully coupled diffusion and stresses in a nonequilibrium Li—Si system by taking into account the effects of composition-dependent modulus, finite concentration, and boundary constraint. The Li-ion diffusion and induced stresses in a bilayer Cu-coated Si anode at the nanometer scale is examined to show these important effects. The transient stress-assisted diffusion problem is solved numerically by a finite difference method, whilst the stress field is obtained analytically. It is shown that the modulus variation with composition plays a mild role in the Li-ion diffusion. In order to account for the finite concentration effect, a nonlinear flux equation is introduced that describes the Li-ion diffusion over the full range of concentration from dilute to near-saturation state in a unified, symmetric manner. The finite concentration effect is significant, especially during the early delithiation process. The boundary constraint effect is found to play an intriguing role in the chemical diffusion. The bending stress results in a resisting force to Li-ion flow preventing effectively the Si anode from full lithiation. The constraint effect is significant for a wide range of Cu thickness.

1. Introduction

Volume changes when a second phase diffuses into or out of a host material. If the volume change occurs nonuniformly or is under a boundary constraint (e.g., a film being bonded to a substrate), stresses are built up in the material. Since the stresses raise mechanical deformation energy, one would intuitively expect the diffusion process that is undertaken to minimize the system free energy to be affected in exchange. In some cases, this chemomechanical coupling effect can be significant. The chemically induced stresses can be so high as to cause severe morphological changes, including fracture. This effect has been held responsible for structural breakdown of active electrode materials and rapid fading of electrochemical device performances. In the wake of searching for new battery electrodes capable of high energy density and high discharge rate, the literature has recently seen a surge of research interest in diffusion induced stresses and fractures [1–39].

The theoretical study of chemoelasticity may be traced back to the early work by Prussin [40]. The follow-on studies have applied the theory to examine the diffusion induced stresses and consequent damage processes including dislocations and fractures [41–45]. Most of these studies have only considered the influence of diffusion on stresses. A few others have included the mutual coupling effects, attempting either to improve the accuracy of an analysis or to interpret interesting phenomena, such as pressure diffusion where the diffusion processes respond to a stress field. Among the recent studies of Li-ion batteries, studies in Refs. [7,15,18,31,32,34,36,37,39] have only considered the diffusion induced stresses. Others [1,2,6,8,19,20,24,30,35,38] have considered the mutual coupling effects. In these studies, insights have been gained into the fracture of active electrode particles and the delamination of active electrode films, especially, the size effect in these critical processes [15,18,30,31,34,36,37]. Atomistic modeling and first-principles calculations have been carried out to understand the underlying physics in the alloying/intercalation processes in electrodes for Li-ion batteries [9,10,16,22,28,29,33,35]. Based on such a bottom-up approach, it was suggested that the modulus of the Li—Si alloy follows the rule of mixtures [28]. This effect quantified by first principles calculations has been

* Corresponding author. Tel.: +1 817 272 9335; fax: +1 817 272 5010.
E-mail address: boyang@uta.edu (B. Yang).

0378-7753/$ – see front matter © 2012 Elsevier B.V. All rights reserved.
doi:10.1016/j.jpowsour.2012.01.029

considered in a continuum mechanics study by a couple of groups [18,35]. Besides all the aforementioned theoretical studies, experimental measurements of stress and modulus [25–27] and direct observations of lithiation processes [21] have been reported. Though scarce, they provided crucial insights into the Li—Si alloying process. The experimental measurements of Young's modulus of $Li_{12}Si_7$ [46] and $Li_{22}Si_5$ [47] altogether with existing data points of pure Si [48] and pure Li [49] confirmed the rule of mixtures being applicable to the Li—Si alloy system in the polycrystalline form (see Fig. 2). However, the magnitudes of the Young's moduli of these alloys significantly differ from the theoretical predictions [28].

The present study is motivated by an attempt to fabricate low-dimensional Si anodes and improve their electronic conductivity. Low-dimensional Si anodes are important to improve the capacity of Li-ion battery, and key to applications such as electrical vehicles that require high power density and high energy density. Free standing Si nanorods/wires/tubes have been fabricated for anode usage in Li-ion batteries [3,13]. Although their performance can be significantly improved relative to that of bulk and thin-film Si materials, they suffer from severe morphological changes over cycles, intensified solid electrolyte interphase buildup in the presence of larger surface/interface area, and rapid capacity fading compared to other types of anodes. To address some of these issues, Cui et al. [11] proposed a carbon nanofiber-Si core–shell structure that may hold the one-dimensional active material together and connect it to the current collector upon fragmentation (as long as the carbon nanotube is connected). An alternative is to partially coat a Si nanorod with a Cu film, or other material combinations [50]. The Cu film would provide structural support to the Si nanorod. Meanwhile, it can improve the electronic conductivity of the anode structure and hence reduce thermal issues.

The present study aims to examine the Li-ion diffusion and stress evolution in a Si nano-anode partially supported by a Cu coating. The Cu film would impose partial constraint on the Si nanorod deformation during the lithiation and delithiation processes. Because Cu is inactive to Li-ion alloying, it would partially insulate the Si nanorod from Li-ion contact and cause uneven Li-ion diffusion on the opposite surfaces of the nanorod. The uneven Li-ion diffusion would result in the nanorod bending, which may or may not be favored for the purpose of stress relief without compromising charge/discharge rate or capacity. During the lithiation/delithiation process, the modulus of the nanorod varies by a couple of tens of times due to the composition change, and the Li-ion diffusion experiences the full range of concentration variation, from dilute to saturated Li-ion concentration. The present study theoretically addresses these effects of composition-dependent modulus, finite concentration and boundary constraint on Li-ion diffusion in a Si nano-anode. Based on the analysis, the following results are worth remarking: (a) a fully coupled chemoelastic analysis of Li-ion alloying with Si showing quantitatively the effects of composition-dependent modulus in the alloying process; (b) introduction of a nonlinear flux equation that describes Li-ion diffusion over the entire range of concentration in a unified, symmetric manner; (c) demonstration of intriguing boundary constraint effect in a bilayer Cu-coated Si anode.

2. Problem formulation

Consider a bilayer Cu-coated Si anode as shown in Fig. 1. The two materials are perfectly bonded at the interface. The Si layer is subjected to Li-ion alloying. Since Cu is inactive to Li-ion alloying, it blocks Li ions from entering the Si layer through the covered surface. It also acts as a structural support to the Si layer. Both of the diffusion and deformation fields are assumed to be one-dimensional through the thickness. The Cartesian coordinate system is established with the x-axis directing along the thickness direction and the origin located at the left boundary, as shown in Fig. 1. There is no constraint for deformation along the z-axis or for bending about the y-axis.

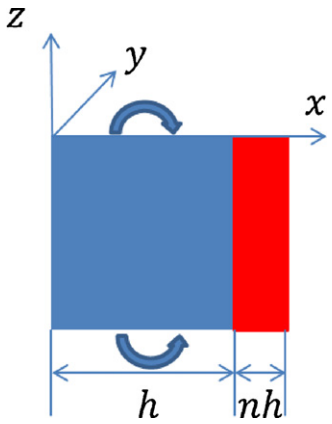

Fig. 1. Schematic showing a bilayer Cu-coated Si anode that is subjected to Li-ion alloying. The diffusion and stress fields are both assumed to be one-dimensional along the x-axis. The composite beam may elongate along the z-axis and bend about the y-axis.

2.1. Equations of chemoelasticity

Within the classical Euler–Bernoulli beam theory, a plane perpendicular to the beam boundary is assumed to remain planar and perpendicular to the beam boundary upon deformation. It results in a linear variation of strain throughout thickness:

$$\varepsilon_z = \varepsilon_{z0} - k_y x, \tag{1}$$

where $\varepsilon_z (\equiv \partial u_z/\partial z)$ is the total strain (the only nontrivial z-component), u_z is the z component of displacement, ε_{z0} is the strain at the boundary ($x = 0$), and k_y is the curvature of the beam. By subtracting the contribution due to inserted Li ions (if any), the elastic strain field is given by

$$e_z = \begin{cases} \varepsilon_{z0} - k_y x - \gamma c & \text{for } 0 < x < h \text{ in Si,} \\ \varepsilon_{z0} - k_y x & \text{for } h < x < (1+n)h \text{ in Cu,} \end{cases} \tag{2}$$

where h is the Si layer thickness, n is the thickness ratio of the Cu layer to the Si layer, c is the Li-ion concentration, and γ is the linear chemical expansion coefficient characterizing dimensional change due to Li-ion insertion in Si. The stress field is given by

$$\sigma_z = \begin{cases} E(\varepsilon_{z0} - k_y x - \gamma c) & \text{for } 0 < x < h \text{ in Si,} \\ E_{Cu}(\varepsilon_{z0} - k_y x) & \text{for } h < x < (1+n)h \text{ in Cu,} \end{cases} \tag{3}$$

where E and E_{Cu} are the Young's moduli of the Li—Si alloy and the Cu layers, respectively. For the sake of brevity, the subscript notation, Li—Si, is omitted for the modulus of Li—Si alloy. The alloy modulus $E(c)$ varies with c, which will be described later. The copper modulus E_{Cu} is a constant. The equilibrium conditions are expressed by

$$\int_0^{(1+n)h} \sigma_z dx = F_z, \tag{4}$$

$$\int_0^{(1+n)h} \sigma_z x dx = M_y - \frac{1}{2} F_z h, \tag{5}$$

where F_z and M_y are the force and couple moment applied at the centroid of the Si layer, respectively. Both of F_z and M_y are set to be zero in later simulations.

Substituting Eq. (3) in Eqs. (4) and (5) and rearranging result in

$$(\bar{E} + E_{Cu}n)\varepsilon_{z0} - \left[\overline{Ex} + \frac{1}{2}E_{Cu}h(n^2+n)\right]k_y = \gamma\overline{Ec} + F_z, \quad (6)$$

$$\left[\overline{Ex} + \frac{1}{2}E_{Cu}h(n^2+n)\right]\varepsilon_{z0} - \left[\overline{Ex^2} + \frac{1}{3}E_{Cu}h^2(n^3+3n^2+3n)\right]k_y = \gamma\overline{Ecx} + M_y. \quad (7)$$

In the above equations, the over-bar denotes an average of the covered function over the Si layer, for example,

$$\overline{Ecx} = \frac{1}{h}\int_0^h Ecx\,dx. \quad (8)$$

Given F_z, M_y and $c(x)$, and given the material constants and geometrical parameters, Eqs. (6) and (7) can be analytically solved to determine ε_{z0} and k_y, with which the stress and strain fields in the composite beam can be fully calculated.

2.2. Equations of mechanochemical diffusion

The Larche–Cahn chemical potential [42] is applied to the Li—Si system:

$$\mu = \mu_0 + RT\ln\frac{c}{c_s - c} - \gamma\sigma_z + \frac{E_{,c}}{2E^2}\sigma_z^2, \quad (9)$$

where R is the universal gas constant, T is the temperature, c_s is the saturation concentration at the stoichiometric limit of $Li_{22}Si_5$, and $E_{,c} \equiv \partial E/\partial c$. The first term μ_0 is invariant of composition. The second term represents the contribution of configurational entropy, where the finite concentration effect is taken into account. The third term is due to the volume change coupled with applied stress. The last term is due to the composition dependence of modulus. Larche [44] suggested that this last term, which is a quadratic function of stress, would be small compared to the preceding term, which is a linear function of stress, because the stress is typically small (relative to E). Sethuraman et al. [27] estimated the last term to be about only 1% in magnitude of the preceding term for the Li—Si system. Later, we will show that the last term can make a mild difference up to 15% in the predicted stresses. Therefore, this last term is kept in our formulation. An interpretation of the discrepancy will be given later with respect to the composition dependence of E.

The Li-ion diffusion flux in Si is assumed to follow a nonlinear law:

$$J = -Mc(1-\hat{c})\frac{\partial\mu}{\partial x}, \quad (10)$$

where M is the Li-ion mobility, and $\hat{c}(\equiv c/c_s)$ is the normalized Li-ion concentration. Compared to the classical flux equation relating to chemical potential gradient [51], the extra modifying factor $(1-\hat{c})$ considers the situation where only those lithium ions with immediate neighboring interstitial sites vacant can migrate. It is also assumed that the probability for a lithium ion finding its immediate neighboring interstitial site vacant is uniform. When c is small, compared to c_s, Eq. (10) is reduced to the common flux equation by neglecting $\hat{c}$ in $(1-\hat{c})$. When c is close to c_s, i.e., when $\hat{c} \approx 1$, Eq. (10) is then reduced to the common flux equation for the diffusion of dilute vacancies at concentration $(c_s - c)$. Recently, Yang et al. [52] identified through a combined experimental and theoretical study that the mobility of interstitial H atoms in Mg and the mobility of H-vacancies in MgH_2 can differ by three orders of magnitude. In the present study of a Li—Si system, it is assumed that the Li-ion mobility is independent of composition. This commonly adopted assumption should be subjected to further examination because a sharp phase boundary between pure Si and its lithiated phase has been observed during the lithiation of a crystalline Si nanowire [3,53] that does not seem to be explainable with this assumption. Although the underlying physics can be different, this speculation of similar composition dependence of Li-ion mobility during the Si lithiation and delithiation is rooted on our recent study of H diffusion in MgH_x with the aforementioned exponential concentration dependence of H mobility and modified Fick's first law given in Eq. (10). It was shown that a sharp phase boundary of Mg hydride can arise during the dehydrogenation process (but not during the hydrogenation process) as a natural result of the exponential concentration dependence of H mobility [54].

By substituting Eq. (9) in Eq. (10), the flux equation is rewritten as

$$J = -MRT\frac{\partial c}{\partial x} - Mc(1-\hat{c})\frac{\partial}{\partial x}\left(\frac{E_{,c}}{2E^2}\sigma_z^2 - \gamma\sigma_z\right). \quad (11)$$

Carrying out the derivative in the second term on the right-hand side and rearranging yield

$$J = -D^*\frac{\partial c}{\partial x} - Mc(1-\hat{c})\left(\gamma E - \frac{E_{,c}}{E}\sigma_z\right)k_y, \quad (12)$$

where D^* is the effective diffusion constant, defined as

$$D^* = \left[1 + \frac{\gamma c_s E}{RT}\hat{c}(1-\hat{c})\left(\gamma - \frac{2E_{,c}}{E^2}\sigma_z + \frac{E_{,cc}}{2\gamma E^3}\sigma_z^2\right)\right]MRT, \quad (13)$$

where $E_{,cc} \equiv (\partial^2 E/\partial c^2)$. The mass conservation equation is given by

$$\frac{\partial c}{\partial t} = -\frac{\partial J}{\partial x}. \quad (14)$$

We impose a boundary condition relating the boundary concentration and flux linearly:

$$J = A(c_{eq} - c)\,\text{at}\,x = 0, \quad (15)$$

$$J = 0\,\text{at}\,x = h, \quad (16)$$

where A is a non-negative rate constant, and c_{eq} is a target (equilibrium) concentration. If c is below c_{eq}, lithium ions flow into the Si layer. In the case when c is above c_{eq}, lithium ions leave the anode. In the process of lithiation, c_{eq} is set to be the saturation concentration c_s. In the reversed process of delithiation, c_{eq} is switched to zero. This condition embraces a rate constant that can be adjusted to impose different charging and discharging rates.

2.3. Materials properties

Most recently Ratchford et al. [46,47] measured the Young's moduli of polycrystalline $Li_{12}Si_7$ and $Li_{22}Si_5$ to be 52 GPa and 35.4 GPa, respectively. Based on the vast literature of Si, the Young's modulus of polycrystalline Si may be assumed to be 170 GPa [48]. Lastly, the Young's modulus of polycrystalline Li was reported to be 8 GPa in an earlier paper [49]. These four data points are plotted versus Li atomic fraction $x/(x+y)$ in Li_xSi_y alloy (where x and y temporarily used here for atomic fraction should not be confused with axes x and y), as shown in Fig. 2. A linear curve fitting is found to approximate well these data points, suggesting the applicability of the rule of mixtures in this case. This behavior is similar to what Shenoy et al. [28] suggested based on their first-principles calculation. However, it should be remarked that their predicted moduli at high Li concentrations are significantly greater in magnitude than the experimental results. The following formula of composition-dependent Young's modulus is used in later simulations:

$$E = 8 + \frac{162}{4.4\hat{c}+1}(\text{GPa}). \quad (17)$$

It recovers exactly the two data points of Si [48] and Li [49] but approximately those of Li—Si alloys [46,47]. More experimental data points are required to affirm Eq. (17).

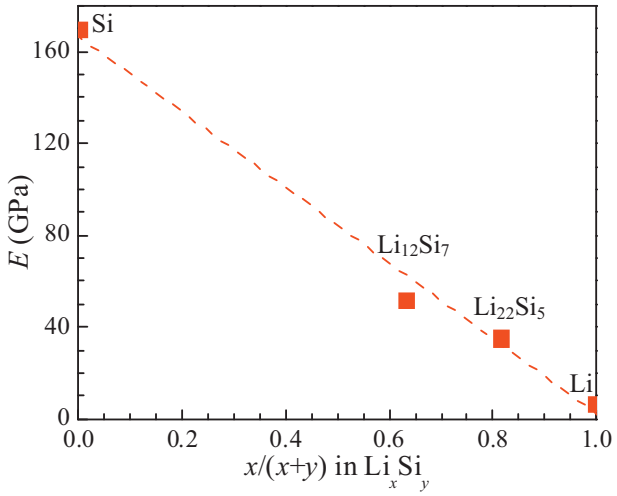

Fig. 2. Variation of Li_xSi_y alloy Young's modulus with Li atomic fraction $x/(x+y)$. The dashed line indicates a linear fitting curve to the data points (symbols).

Based on the volume and space groups of a few intermediate crystalline phases of Li_xSi_y alloy given in Table 1 in Ref. by Shenoy et al. [28], we plotted the variation of alloy volume per Si atom as a function of composition ratio x/y, as shown in Fig. 3. It shows that the alloy volume is nearly a linear function of x/y. In the present study, the Li-ion concentration c is defined as the amount of Li-ion per unit initial volume. Thus, c is proportional to composition ratio x/y. Based on this graph, the chemical expansion coefficient, γ can be reasonably assumed to be a constant, and is estimated to be $1.64 \times 10^{-6}\,m^3\,mol^{-1}$. The saturation concentration c_s is defined at the stoichiometric limit of $Li_{22}Si_5$, which is equal to $3.65 \times 10^5\,mol\,m^{-3}$. The value of diffusion constant D equal to $10^{-13}\,m^2\,s^{-1}$ is taken from Ref. [5]. It can differ by orders of magnitude according to other Refs. [12,14,22,55]. The Young's modulus of copper is equal to 128 GPa. In latter simulations, the Si thickness h is fixed at 100 nm. The temperature T is fixed at 300 K.

It may be worth noting that there have been theoretical and experimental studies suggesting that amorphous Zintl phase compounds occur during the lithiation and delithiation processes of Si regardless of its initial crystalline or amorphous state [56–60]. Thus, the actual variations of elastic moduli and volume can be more complicated than what are depicted in Figs. 2 and 3. This is also why

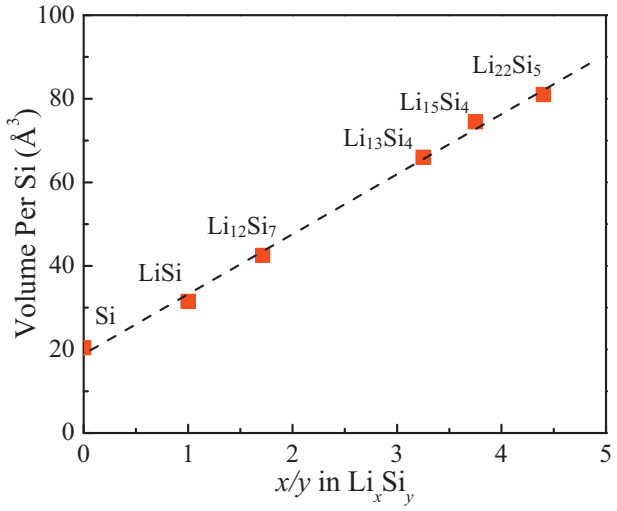

Fig. 3. Variation of Li_xSi_y alloy volume per Si atom with composition ratio x/y. The dashed line indicates a linear fitting curve to the data points (symbols).

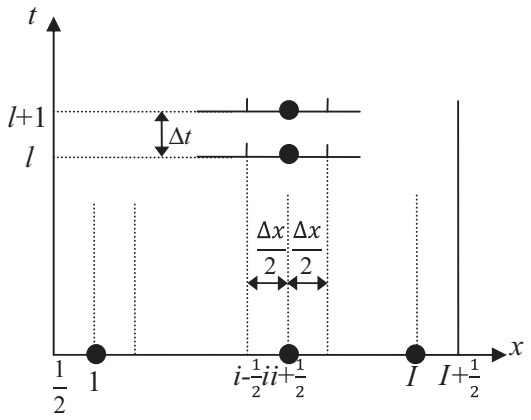

Fig. 4. Schematic showing a finite difference discretization of the x and time axes.

the data points of crystalline Li—Si alloys were connected by dotted lines in these figures. A detailed consideration of this effect, as well as of the aforementioned possible strong composition dependence of Li-ion mobility, is beyond the scope of the present work, and is left to a future study.

3. Finite difference method for stress-assisted diffusion

An analytical expression of stress has been derived above for a bilayer beam, with a Li-ion concentration field as a loading source. However, the diffusion problem is nonlinear and can only be solved numerically. A finite difference method is adopted to approximate the transient differential equations of diffusion. The analytical expressions of stress and the numerical finite difference equations of diffusion are combined to solve the coupled diffusion and stress evolution in time. The numerical scheme is summarized below.

The Si layer is discretized in I equal divisions along the x axis, as shown in Fig. 4. A node is defined at the middle point of each division, and is numbered by $1, 2, \ldots, i, \ldots, I$. The axis of time is discretized unevenly, with time step Δt to be determined by current value of effective diffusion constant D^* as well as nodal spacing Δx ($=h/I$).

The mass conservation equation, Eq. (14), is approximated by

$$c_i^{l+1} - c_i^l = -\frac{\Delta t}{\Delta x}\left(J_{i+\frac{1}{2}}^{l+1} - J_{i-\frac{1}{2}}^{l+1}\right), \text{ for } i = 1, 1, \ldots, I \tag{18}$$

where l indicates the lth time step. The time increment Δt is determined by $\alpha \Delta x^2 / D^*_{max}$, where D^*_{max} is the maximum nodal value of D^* at the previous time step l, and α is a numerical stability control parameter, set to be $\alpha = 1$ in later simulations.

The flux equation, Eq. (12), is approximated by

$$J_{i+\frac{1}{2}}^{l+1} = -\frac{D_i^{*l} + D_{i+1}^{*l}}{2\Delta x}\left(c_{i+1}^{l+1} - c_i^{l+1}\right) - \frac{1}{2}(K_i^l + K_{i+1}^l), \text{ for } i = 1, \ldots, I-1, \tag{19}$$

where $K = Mc(1-\hat{c})(\gamma E - (E_{,c}/E)\sigma_z)k_y$.

The boundary conditions at $i = 1/2$ and $I + 1/2$ are approximated/given by

$$J_{\frac{1}{2}}^{l+1} = A(c_{eq}^{l+1} - c_1^{l+1}), \tag{20}$$

$$J_{I+\frac{1}{2}}^{l+1} = 0. \tag{21}$$

Note that in the special case that the Cu-layer is absent, the problem is symmetric. Only one half of the Si layer needs to be considered, and the same boundary conditions as above (Eqs. (20) and (21)) can be applied at the two effective ends.

The solution procedure is the following. Given the concentration field at the lth time step, the Si modulus and its derivatives are calculated according to Eq. (17). Then, ε_{z0} and k_y are obtained by solving Eqs. (6) and (7), which leads to determination of the stress field. Then, the effective diffusion constant D^* is calculated together with the bending-induced flux K. Finally one can assemble a system of algebraic equations, by submitting Eqs. (19)–(21) into Eq. (18), and solve for nodal concentration $c_i^{l+1}(i = 1, 2, \ldots, I)$ at a current time step $l+1$. The process is repeated to obtain the diffusion and stress fields in time.

4. Numerical results and discussion

This section presents the simulations based on the method described above and examines the effects of the composition-dependent modulus, the finite concentration (Eq. (10)) and the boundary constraint on lithiation/delithiation of a Si and a Cu-coated Si nanorod. Two hundred divisions are used to discretize the anode domain. The stability control parameter α is set to be one in determining each time increment by $\Delta t = \alpha \Delta x^2 / D^*_{\max}$, where $D^*_{\max}$ is the maximum effective diffusion constant at a time step. During the simulations, c_{eq} is initially set to be c_s for the lithiation. When the total Li-ion insertion reaches 99% of the total saturation amount, it is reset to be zero. Upon that, the delithiation process begins. Other than this switch, the solution procedure is identical in the processes of lithiation and delithiation. The rate constant A in the boundary condition (Eq. (15)) is set to be 10^{-5} m s^{-1} for all cases examined. The numerical convergence was achieved with the above mesh; doubling the mesh density, there was observed little change to any of the results presented in the figures below.

4.1. Effects of composition-dependent modulus

At first, a set of three simulations is performed in the absence of a Cu layer. Thus, the problem is symmetric, and the Si anode stays straight (i.e., no bending). In this case, only one half of the problem needs to be considered, as discussed before. In the first simulation, all of the composition-dependent modulus E and its derivatives $E_{,c}$ and $E_{,cc}$, involved in the above diffusion equations, are kept in the calculation. In the second simulation, only the composition-dependent modulus E is kept, but all of its derivatives are set equal to zero. In the last simulation, the modulus E is set to be a constant equal to the modulus of Si. Consequently, all of its derivatives are equal to zero. In these simulations, the total Li-ion amount in the Si anode is recorded over time. The maximum and minimum stresses in the anode are recorded at every time step. Note that the maximum and minimum stresses shift in position over time. They indicate the severity of stressing that the anode would experience during the lithiation and delithiation processes. The results are plotted in Figs. 5 and 6, respectively. Fig. 5 shows the variation of Li-ion uptake over time. Fig. 6(a) shows the variation of maximum and minimum stresses over the lithiation and delithiation processes. Fig. 6(b) shows the variation of the same quantities over an early short period of time. In these figures and all other figures in the following, all quantities of the dimension of time are normalized by characteristic diffusion time $t_c = h^2/D$. All quantities of the dimension of length are normalized by h. All quantities of the dimension of stress are normalized by E_{Si}, the modulus of pure silicon. All quantities of the dimension of concentration are normalized by saturation concentration c_s at the stoichiometric limit.

From Figs. 5 and 6, it can be seen that both the Li-ion insertion and extraction proceed at relatively high rate initially and then gradually slow down. It results in high stress shortly after the beginning of lithiation or delithiation. The stress decays gradually afterwards. These characteristic behaviors reflect the imposed boundary condition.

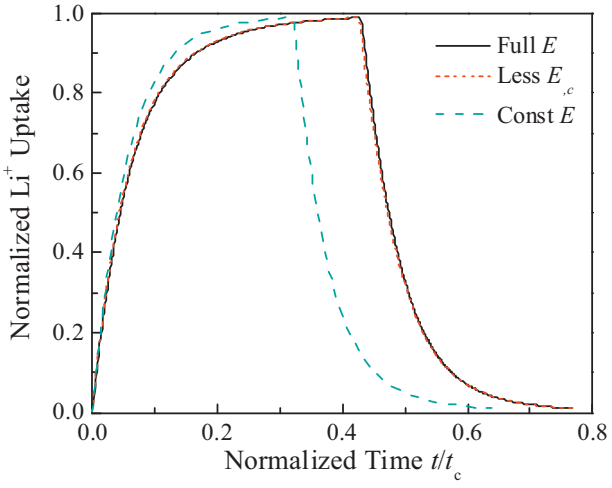

Fig. 5. Variation of Li-ion uptake (normalized by saturation amount) with time. Legend "Full E" indicates the case with effects of composition-dependent alloy modulus fully taken into account. Legend "Less $E_{,c}$" indicates the case with alloy modulus varying but its derivatives being set to be zero in the diffusion equations. Legend "Const E" indicates the case of constant alloy modulus, set to be that of pure Si.

Compare the results of the three cases of fully considered composition-dependent modulus, derivative-less composition-dependent modulus, and constant modulus, which are indicated by "Full E", "Less $E_{,c}$" and "Const E", respectively, in Fig. 5. It can be seen that the composition-dependent modulus plays a significant role in determining the diffusion process as well as the stress field. The effect of the modulus derivative is mild. The diffusion curves in Fig. 5 are nearly identical in those two cases of varying modulus. However, in Fig. 6, one can see that the exclusion of modulus derivatives

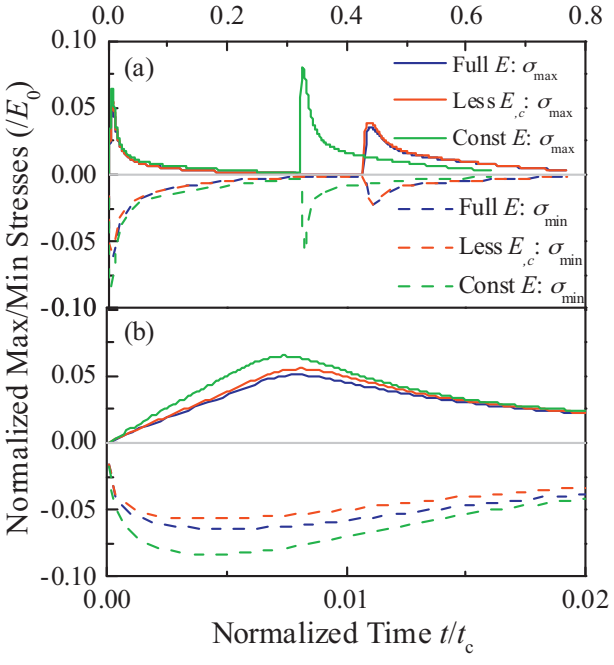

Fig. 6. Variations of maximum (solid) and minimum (dotted) stresses with time: (a) full lithiation and delithiation process; (b) early short period. Legend "Full E" indicates the case with effects of composition-dependent alloy modulus fully taken into account. Legend "Less $E_{,c}$" indicates the case with alloy modulus varying but its derivatives being set to be zero in the diffusion equations. Legend "Const E" indicates the case of constant alloy modulus equal to that of pure Si.

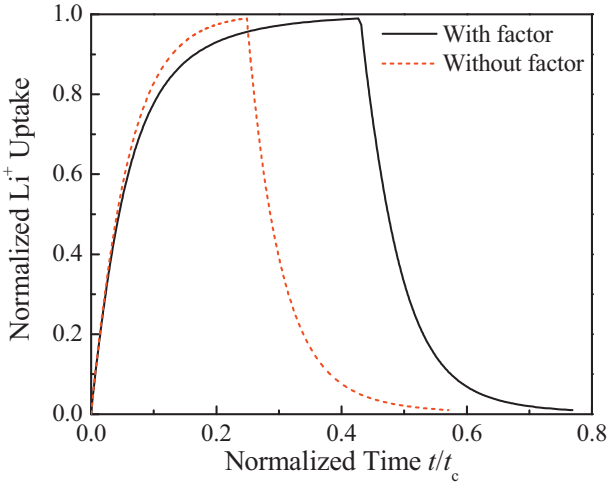

Fig. 7. Variation of Li-ion uptake (normalized by saturation amount) with time. Legends "With factor" and "Without factor" indicate the cases with and without modification factor $(1-\hat{c})$ in the flux equation, respectively.

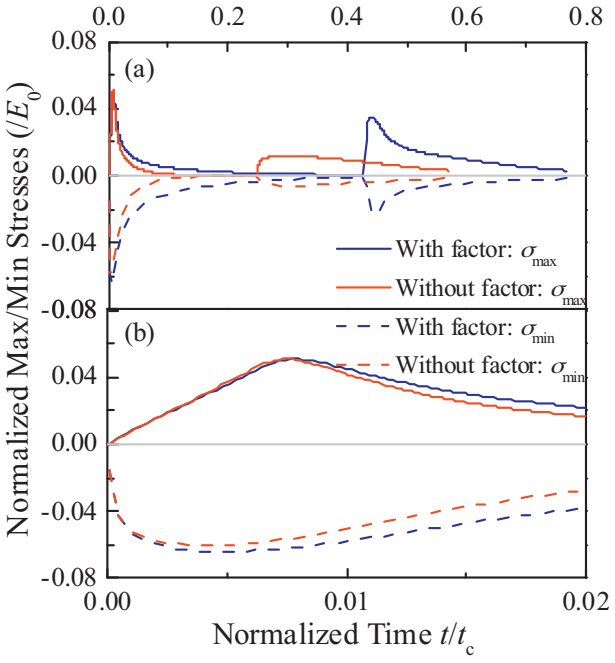

Fig. 8. Variations of maximum (solid) and minimum (dotted) stresses in Si with time: (a) full lithiation and delithiation process; (b) early short period. Legends "With factor" and "Without factor" indicate the cases with and without modification factor $(1-\hat{c})$ in the flux equation, respectively.

in the calculation makes a mild difference up to 15% in the predicted maximum stresses. This is in contrast to the estimate of 1% difference (in potential) made by Sethuraman et al. [27] We attribute the mild difference to the softening composition-dependent modulus and to the (elastic) stress magnitude we allowed to reach up to ~6% of E_{Si} in view of the possible high yield strength up to 7–10 GPa in Si [61,62] compared to its modulus of 170 GPa and the measured flow stress of 1.5 GPa in $Li_{15}Si_4$ by Sethuraman et al. [25] compared to the measured Young's modulus of 35 GPa in Li_3Si by Sethuraman et al. [26] Note that the significance of the terms involving $E_{,c}$ is determined by the ratio of stress to the Young's modulus (Eq. (13)).

4.2. Effects of flux equation modification/finite concentration

Then, a simulation is run where the classical flux equation is applied by removing factor $(1-\hat{c})$ from Eq. (10). All other considerations are kept the same as above. The same results, i.e., variations of Li-ion uptake and maximum and minimum stresses over time, are acquired in the simulation, and are plotted in Figs. 7 and 8.

From Figs. 7 and 8, it can be clearly seen that this modification factor $(1-\hat{c})$ applied to the classical flux equation makes a significant difference in the diffusion process, especially in the delithiation process. Although the predicted stresses are about the same during the lithiation process, during the delithiation process the predicted maximum and minimum stresses by the classical flux equation are only about one third of those predicted by the modified law. This is expected because the effective diffusion constant is much lowered at high concentrations by the modification. With the same rate constant of insertion and extraction at the boundary, the diffusion field is less steep and thus the stresses are lower at high concentrations within the classical formulation. We believe that the present formulation with the modified flux equation is more physically reasonable. It characterizes the early stages of lithiation and delithiation in a unified, symmetric manner. It predicts the early processes of lithiation and delithiation with about the same magnitudes of stresses and about the same diffusion characteristics. The present modification symmetrizes the description of the lithiation and delithiation processes. If these two opposite processes are different, we suggest that it should be caused by their different material properties, for instance, due to different mobility of Li-ion migration in Si and in $Li_{4.4}Si$, not by the law.

4.3. Effects of boundary constraint–Cu coating

Finally, a set of simulations is performed with various Cu-layer thicknesses in order to investigate the constraint effect of a Cu layer bonded to one side of the Si anode. The full model is considered, including the effects of composition-dependent modulus and its derivatives and the flux equation modification. Because copper is inactive to Li-ion alloying, the Cu layer effectively blocks Li-ion from flowing through the coated surface area of the Si anode. As discussed before, it would lead to the anode bending and hence asymmetric diffusion and stress fields. The variations of Li-ion uptake and maximum and minimum stresses in the anode are recorded over time. Also the variation of anode bending curvature is recorded over time. Since the characteristics of the Li-ion uptake variation are the same as before and since the time scales involved can be viewed from the other profiles, only the stress and bending curvature variations are plotted in Figs. 9 and 10.

Fig. 9(a)–(d) shows the variations of maximum and minimum stresses in the anode over time. This is done for four particular cases: Cu-layer thickness equal to 0 (trivial thickness), 1 nm, 100 nm, and 1 μm. Figs. 10(a)–(d) shows the variations of anode bending curvature over time in the same four cases. Recall that the anode thickness is 100 nm. The Cu modulus of 128 GPa is roughly three quarters of the crystalline Si modulus, and roughly three and half times the full alloy ($Li_{22}Si_5$) modulus. From these figures, it can be seen that the time scale involved in the lithiation process is very sensitive to the Cu thickness when it is close to the anode thickness. The time to finish 99% of the lithiation initially increases with Cu thickness, reaches a peak, and finally decreases with further increase of Cu thickness.

When the Cu-layer thickness is trivial (Figs. 9a and 10a), the Si anode starts to bend as soon as the lithiation process begins. After a short period of time, it reaches its maximum curvature and then gradually recovers from bending. The Cu-layer of trivial thickness blocks the Li-ion flow on the right boundary of the anode, but has no mechanical constraint effect on the anode flexural deformation.

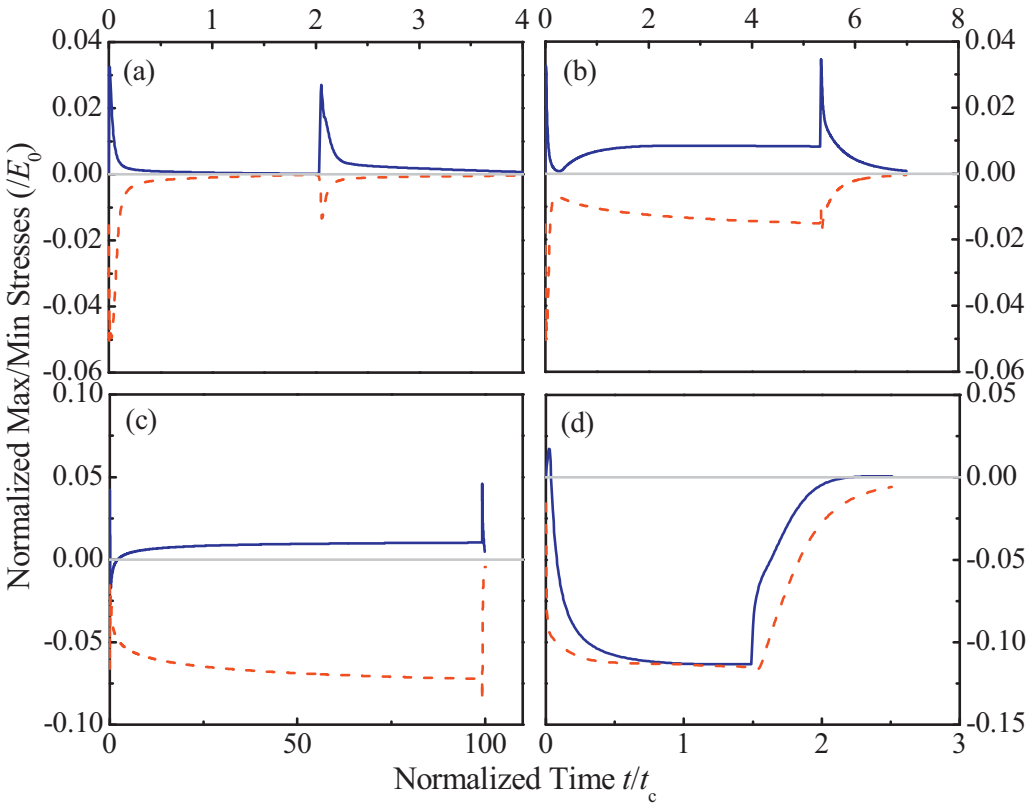

Fig. 9. Variations of maximum (solid) and minimum (dotted) stresses in Si with time at various Cu-layer thicknesses: (a) 0; (b) 1 nm; (c) 100 nm; and (d) 1 μm.

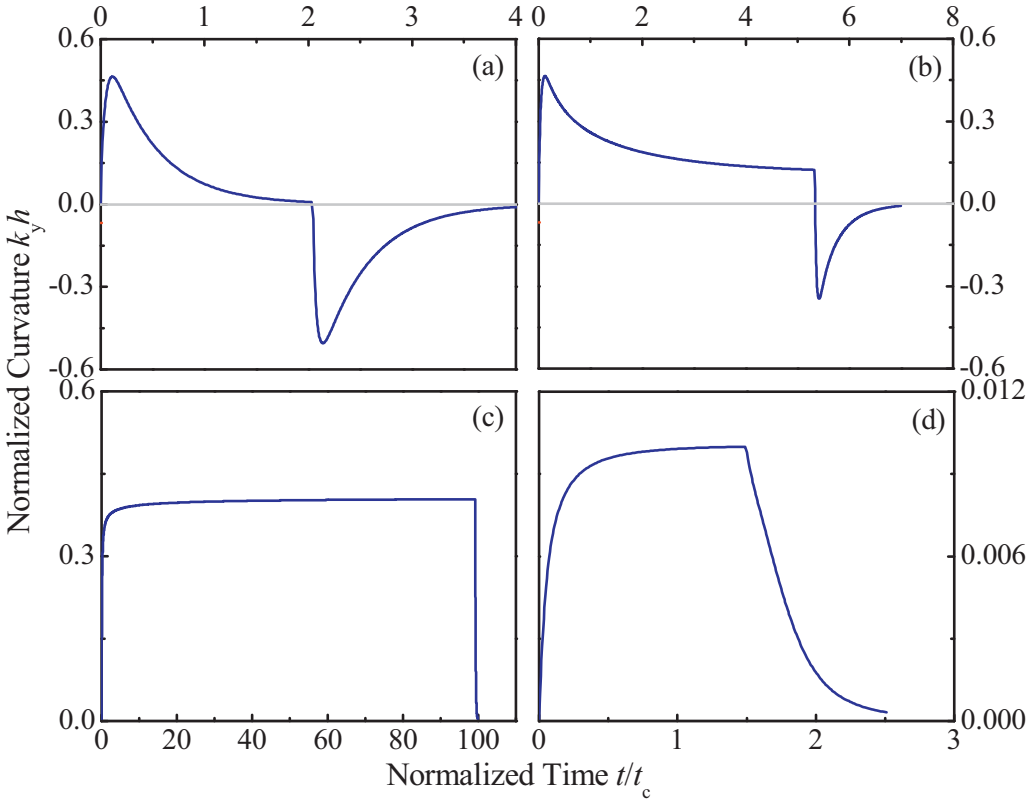

Fig. 10. Variations of anode bending curvature with time at various Cu-layer thicknesses: (a) 0; (b) 1 nm; (c) 100 nm; and (d) 1 μm.

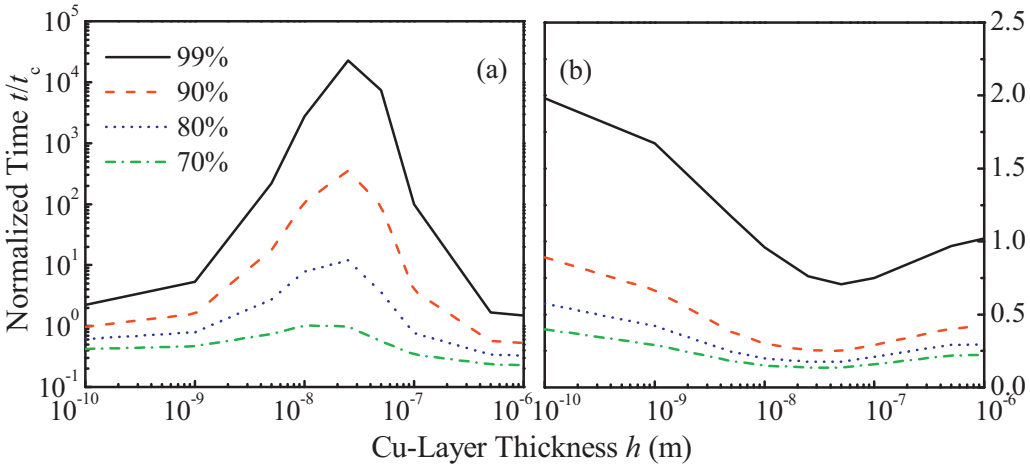

Fig. 11. Variations of (a) charging and (b) discharging times at various percentages of completeness (Li-ion uptake normalized by saturation amount) with Cu-layer thickness.

The resulting nonuniform concentration field causes the anode to bend. In the fully charged state, the concentration field returns uniformity, and the anode recovers its original straight configuration. The maximum and minimum stresses, which are tensile and compressive, respectively, spike at the early time but quickly decay along with the lithiation process. When discharging, the behavior is characteristically similar to the above case of charging, except that everything switches sign.

When the Cu-layer thickness is equal to 1 nm (Figs. 9b and 10b), which is one hundredth of the anode thickness, substantial effects are seen in the stress and deformation results. The anode response is about the same as above in the early period of time. When the lithiation process continues, the bending curvature and the maximum and minimum stresses all decrease. However, upon full lithiation, the composite structure remains bent appreciably, and the resulting stresses in the anode remain high. The time needed for full lithiation is more than doubled, relative to the above case of trivial thickness. In contrast, the Cu layer of thickness equal to 1 nm has minor effect on the delithiation process. These observations can only be explained by invoking that the 1-nm thick Cu layer plays a significant role in both of the diffusion and deformation processes in the Si anode layer.

When the Cu-layer thickness is equal to 100 nm (Figs. 9c and 10c), the diffusion and deformation processes continue to change relative to the previous cases. The time needed to fully charge the anode is more than an order of magnitude longer than that in the first case of trivial Cu-layer thickness. The maximum and minimum stresses are both reduced, indicating that the constraint of a thicker Cu-layer holds the anode in more compressive state than the above cases of nearly free-standing anode due to the Li-ion insertion. The bending curvature rapidly increases initially but varies very slowly afterwards, indicating that the composite structure has nearly reached a lock-up state of deformation. The internal stresses only vary slowly in correspondence. This also indicates that the diffusion process evolves very slowly in the nearly lock-up state. The above observations are more pronounced when the Cu-layer thickness is 10 nm, which is also examined but is not shown here.

When the Cu-layer thickness is increased to 1 μm (Figs. 9d and 10d), the composite structure behaves effectively like a thin film bonded to a thick substrate. The bending curvature is nearly zero during the entire lithiation and delithiation process. The maximum and minimum stresses are nearly the same and are both compressive. It means essentially that the anode is fully constrained by the Cu layer. Interestingly, the charging time is on the same order of magnitude as in the case of trivial constraint.

In order to better understand the constraint effect at various charging and discharging stages, the time needed to charge/discharge 70%, 80%, 90% and 99% is recorded. This is done for various Cu-layer thicknesses. The results are shown in Fig. 11a and b, for charging and discharging, respectively. It can be seen from Fig. 11a that between 1 nm and 1 μm of Cu-layer thickness, the charging time increases substantially, especially for high charging percentages. The peak can be a few orders of magnitude longer than that of either trivial or very thick Cu-layer support. In contrast, the Cu-layer constraint effect has relatively little effect on the discharging process in the entire range of examined Cu-layer thicknesses. By examining Eq. (12) and Fig. 11a and b, it may be remarked that the term independent of concentration gradient but proportional to bending curvature in Eq. (12) is always opposing to the Cu layer. In the lithiation process, it can lead to a lock-up state, effectively blocking the anode from full charging. In contrast, in the reversed delithiation process, this term assists the Li-ion diffusion out of the anode, which is clearly seen in Fig. 11b.

5. Conclusions

A fully coupled chemoelastic analysis has been carried out for lithiation and delithiation of a bilayer Cu-coated Si anode. The classical Larche–Cahn chemical potential [42] was adopted to describe the Li—Si alloy system. The term of chemical potential due to elastic modulus variation with composition is kept in order to evaluate its effect on Li-ion diffusion. A nonlinear flux equation is introduced that symmetrizes the law for Li-ion diffusion at dilute and near-saturation concentrations. Meanwhile, the deformation and stress chemically induced by Li-ion insertion in the bilayer composite structure are modeled within the classical beam theory and solved analytically. The stress-assisted diffusion problem is nonlinear and is solved numerically by applying a finite difference method.

It has been shown that the effects of composition-dependent Li—Si alloy modulus are significant on the stress field but less significant on the diffusion process. The second derivative of modulus with respect to composition can be safely omitted from the diffusion equation. In contrast, the first derivative can make a mild difference up to 15% in predicted maximum stresses with and without it. Also, it has been shown that the flux equation modification can make a significant difference, especially, during the delithiation process. The modified flux equation is considered as more reasonable when applying to the whole range of concentration from dilute to near saturation. It describes the Li-ion diffusion at dilute and near-saturation concentrations in a unified, symmetric manner.

Finally, it has been shown that the Cu layer on one side of the Si anode can play a profound role, not only in blocking surface Li-ion flux, but also in substantiating a term of bending curvature in the flux equation opposing Li-ion insertion into the anode. This term due to bending stress gradient can effectively hold the anode from full lithiation for a range of Cu-layer thickness, but can also somewhat accelerate the delithiation process.

Acknowledgement

This work was supported by US Army with the contract number of W911NF-10-2-0107.

References

[1] J. Christensen, J. Newman, Journal of The Electrochemical Society 153 (6) (2006) A1019.
[2] J. Christensen, J. Newman, Journal of Solid State Electrochemistry 10 (5) (2006) 293–319.
[3] C.K. Chan, et al., Nature Nanotechnology 3 (1) (2007) 31–35.
[4] Z.H. Jin, Journal of Applied Physics 102 (8) (2007) 083533.
[5] K. Yoshimura, et al., Journal of Power Sources 174 (2) (2007) 653–657.
[6] X. Zhang, W. Shyy, A. Marie Sastry, Journal of the Electrochemical Society 154 (10) (2007) A910.
[7] Y.-T. Cheng, M.W. Verbrugge, Journal of Applied Physics 104 (8) (2008) 083521.
[8] X. Zhang, A.M. Sastry, W. Shyy, Journal of the Electrochemical Society 155 (7) (2008) A542.
[9] V.L. Chevrier, J.R. Dahn, Journal of the Electrochemical Society 156 (6) (2009) A454.
[10] V.L. Chevrier, J.W. Zwanziger, J.R. Dahn, Canadian Journal of Physics 87 (6) (2009) 625–632.
[11] L.-F. Cui, et al., Nano Letters 9 (9) (2009) 3370–3374.
[12] N. Ding, et al., Solid State Ionics 180 (2-3) (2009) 222–225.
[13] M.H. Park, et al., Nano Letters 9 (11) (2009) 3844–3847.
[14] R. Ruffo, et al., Journal of Physical Chemistry C 113 (26) (2009) 11390–11398.
[15] Y.-T. Cheng, M.W. Verbrugge, Journal of the Electrochemical Society 157 (4) (2010) A508.
[16] V.L. Chevrier, J.R. Dahn, Journal of the Electrochemical Society 157 (4) (2010) A392.
[17] J. Christensen, Journal of the Electrochemical Society 157 (3) (2010) A366.
[18] R. Deshpande, Y. Qi, Y.-T. Cheng, Journal of the Electrochemical Society 157 (8) (2010) A967.
[19] S. Golmon, et al., Applied Physics Letters 97 (3) (2010) 033111.
[20] H. Haftbaradaran, H. Gao, W.A. Curtin, Applied Physics Letters 96 (9) (2010) 091909.
[21] J.Y. Huang, et al., Science 330 (6010) (2010) 1515–1520.
[22] B. Peng, et al., The Journal of Chemical Physics 133 (3) (2010) 034701.
[23] Y. Qi, S.J. Harris, Journal of the Electrochemical Society 157 (6) (2010) A741.
[24] S. Renganathan, et al., Journal of the Electrochemical Society 157 (2) (2010) A155.
[25] V.A. Sethuraman, et al., Journal of Power Sources 195 (15) (2010) 5062–5066.
[26] V.A. Sethuraman, et al., Electrochemistry Communications 12 (11) (2010) 1614–1617.
[27] V.A Sethuraman, et al., Journal of the Electrochemical Society 157 (11) (2010) A1253.
[28] V.B. Shenoy, P. Johari, Y. Qi, Journal of Power Sources 195 (19) (2010) 6825–6830.
[29] W. Wan, et al., Journal of Physics: Condensed Matter 22 (41) (2010) 415501.
[30] W.H. Woodford, Y.-M. Chiang, W.C. Carter, Journal of the Electrochemical Society 157 (10) (2010) A1052.
[31] F. Yang, Journal of Applied Physics 108 (7) (2010) 073536.
[32] F. Yang, Journal of Applied Physics 107 (10) (2010) 103516.
[33] Q. Zhang, et al., Nano Letters 10 (9) (2010) 3243–3249.
[34] K. Zhao, et al., Journal of Applied Physics 108 (7) (2010) 073517.
[35] H. Haftbaradaran, et al., Journal of Power Sources 196 (1) (2011) 361–370.
[36] X. Xiao, et al., Journal of Power Sources 196 (3) (2011) 1409–1416.
[37] F. Yang, Journal of Power Sources 196 (1) (2011) 465–469.
[38] W.L. Wang, S. Lee, J.R. Chen, Journal of Applied Physics 91 (12) (2002) 9584.
[39] R.E Garcıïa, et al., Journal of the Electrochemical Society 152 (1) (2005) A255.
[40] S. Prussin, Journal of Applied Physics 32 (10) (1961) 1876–1881.
[41] J. Chen-Min Li, Metallurgical and Materials Transactions A 9 (10) (1978) 1353–1380.
[42] F.C. Larche, J.W. Cahn, Acta Metallurgica 33 (3) (1985) 331–357.
[43] I.V. Belova, G.E. Murch, Journal of Applied Physics 77 (1) (1995) 127–134.
[44] F.C. Larché, Le Journal de Physique IV 6 (C1) (1996), C1-03–C1-09.
[45] M.V. Paukshto, International Journal of Fracture 97 (1–4) (1999) 227–236.
[46] J.B. Ratchford, unpublished.
[47] J.B. Ratchford, et al., Journal of Power Sources 196 (18) (2011) 7747–7749.
[48] W.N. Sharpe, et al., MEMS 97, Proceedings – IEEE the Tenth Annual International Workshop on Micro Electro Mechanical Systems: An Investigation of Micro Structures, Sensors, Actuators, Machines and Robots, 1997, pp. 424–429.
[49] W. Robertson, D. Montgomery, Physical Review 117 (2) (1960) 440–442.
[50] L.Q. Zhang, et al., ACS Nano 5 (6) (2011) 4800–4809.
[51] P. Shewmon, Diffusion in Solids, 2nd ed., TMS, Warrendale, PA, 1989.
[52] B. Yang, Y.P. He, Y.P. Zhao, Applied Physics Letters 98 (8) (2011) 081905.
[53] X.H.et al. Liu, Nano Letters (2011).
[54] B. Yang, Y. He, Y. Zhao, International Journal of Hydrogen Energy 36 (24) (2011) 15642–15651.
[55] E.M. Pell, Physical Review 119 (4) (1960) 1222.
[56] M. Green, et al., Electrochemical and Solid-State Letters 6 (5) (2003) A75.
[57] V.L. Chevrier, J.W. Zwanziger, J.R. Dahn, Journal of Alloys and Compounds 496 (1–2) (2010) 25–36.
[58] C.-Y. Chou, H. Kim, G.S. Hwang, The Journal of Physical Chemistry C 115 (40) (2011) 20018–20026.
[59] H. Kim, et al., The Journal of Physical Chemistry C 115 (5) (2011) 2514–2521.
[60] R. Nesper, Progress in Solid State Chemistry 20 (1) (1990) 1–45.
[61] G.T.A. Kovacs, Micromachined Transducers Sourcebook, WCB/McGraw-Hill, 1998.
[62] Z. Yang, Z. Lu, Y.-P. Zhao, Journal of Applied Physics 106 (2) (2009) 023537.